Sciencexpress Reports

# Mechanisms of antiwear tribofilm growth revealed in situ by single-asperity sliding contacts

**N. N. Gosvami,[1] J. A. Bares,[1]* F. Mangolini,[2] A. R. Konicek,[3] D. G. Yablon,[3]† R. W. Carpick[1]‡**

[1]Department of Mechanical Engineering and Applied Mechanics, University of Pennsylvania, Philadelphia, PA 19104, USA. [2]Department of Materials Science and Engineering, University of Pennsylvania, Philadelphia, PA 19104, USA. [3]Corporate Strategic Research, ExxonMobil Research and Engineering, Annandale, NJ 08801, USA.

*Present address: BorgWarner Powertrain Technical Center, Auburn Hills, MI 48326, USA.

†Present address: SurfaceChar LLC, Sharon, MA 02067, USA.

‡Corresponding author. E-mail: carpick@seas.upenn.edu

**Zinc dialkyldithiophosphates (ZDDPs) are widely used additives in automotive lubricants which form crucial antiwear tribofilms at sliding interfaces. The mechanisms governing the tribofilm growth are not well-understood, limiting the development of replacements with better performance and catalytic converter compatibility. Using atomic force microscopy in ZDDP-containing lubricant base stock at elevated temperatures, we monitor the growth and properties of the tribofilms in situ in well-defined single-asperity sliding nanocontacts. Surface-based nucleation, growth, and thickness saturation of patchy tribofilms are observed versus sliding time. The growth rate increases exponentially with either applied compressive stress or temperature, consistent with a thermally-activated, stress-assisted reaction rate model. The films grow regardless of the presence of iron on either the tip or substrate, highlighting the critical role of stress and thermal activation.**

Additives are crucial components of lubricants used in a wide range of tribological applications including vehicles, turbines, and manufacturing equipment (*1*). Additives such as friction modifiers and antiwear additives are particularly important, as they have widespread impact, including considerably reducing global energy and material consumption, and extending many industrial and automotive application lifetimes by orders of magnitude. One of the most crucial modern antiwear additives is zinc dialkyldithiophosphate (ZDDP), (chemical formula $Zn[S_2P(OR)_2]_2$, with R being an alkyl group, which is often varied) (*2*, *3*) (fig. S2). Based on extensive macroscopic studies, ZDDP molecules are understood to decompose at rubbing interfaces (*4*, *5*) and form protective surface-bonded tribofilms that dramatically reduce wear by minimizing metal-to-metal contact of steel and iron (*3*), and other material pairs (*6*, *7*). ZDDP-derived tribofilms consist of rough, patchy, pad-like features that are composed of pyro- or ortho-phosphate glasses in the bulk with an outer nanoscale-layer of zinc polyphosphates and a sulfur-rich layer near the metal surface (*3*). However, the tribochemical film growth pathways are not established, and the factors which determine the film morphology and thickness (which tends to be limited to 50-150 nm) are unknown (*3*). Furthermore, ZDDP's effectiveness as an antiwear additive for advanced engine materials is not yet clear. For low-weight materials (*e.g.*, Al- and Mg-based alloys), ZDDP forms robust tribofilms primarily on load-bearing inclusions, but not on surrounding softer matrices (*6*, *8*). While ZDDP tribofilms can be formed between other non-ferrous material pairs, *e.g.*, low-friction diamond-like carbon (DLC) films, they are often less durable than those formed when steel or iron is present for reasons not yet understood (*9*, *10*). It is desirable to reduce or replace ZDDP as it often increases frictional losses (*3*), and produces Zn-, P- and S-containing compounds in the exhaust, reducing the catalytic converter's efficiency and lifetime (*1*, *3*, *11*, *12*). Despite decades of research, no suitable substitute for ZDDP has yet been found (*12*), motivating research to understand the beneficial mechanisms underlying the growth and antiwear properties of ZDDP-derived tribofilms.

A range of macroscopic methods have been developed to produce ZDDP tribofilms (*13*, *14*), and the resulting films have been studied by many ex situ mechanical and chemical approaches (*3*, *15*) and atomistic simulations (*8*). It is widely assumed that the tribofilm acts as a protective layer that is continually replenished, reducing metal-to-metal contact (*3*). Although some studies indicate that antiwear properties arise due to ZDDP's ability to reduce peroxides in the base stock, preventing corrosion (*16*, *17*). One model explaining ZDDP tribofilm formation on steel is based on hard and soft acid base (HSAB) reactions (*18*), which require the exchange of $Zn^{2+}$ and $Fe^{3+}$ cations between the ZDDP and iron oxide wear particles respectively, where the latter are digested within the tribofilm (*19*). Direct experimental evidence for this model is lacking (*3*), and it does not explain tribofilm formation on non-ferrous surfaces (*6*, *7*). In contrast, Mosey *et al.*'s first principles atomistic simulations proposed that tribofilm formation results from contact pressure-induced cross-linking of zinc phosphate molecules (*8*) which are a thermal or catalytic decomposition product of ZDDP (*11*, *15*).

Overall, there is no consensus on the growth mechanism, and no models conclusively explain either the tribofilm patchiness or why the film thickness is limited. All prior experiments have been conducted for macroscopic, multi-asperity contacts (specific asperity contact areas and pressures thus being unknown) that are then analyzed post mortem and ex situ, often after extracting the sample from base stock, potentially altering the tribofilm (*20*). Although macroscopic in situ studies of zinc polyphosphates under static compression (*21*, *22*) have shown irreversible loss of crystallinity and little increase in polymerization with increased pressure, these studies do not involve dynamic sliding. In situ single-asperity sliding studies have the advantage that contact loads and geometries can be controlled and quantified, local tribofilm properties such as morphological evolution with nanometer resolution, tribofilm volume, friction, adhesion and wear measured concurrently, and results compared with atomistic simulations (*8*).

Single-asperity studies are conducted here with an atomic force microscope (AFM), where the AFM tip is slid against an Fe-coated or uncoated Si substrate at temperatures up to 140°C while immersed in ZDDP-containing base stock (*23*) to dynamically generate the tribofilm (fig. S3). Low-load (10-20 nN) contact mode imaging reveals a soft, weakly-bound thermal film formed without prior sliding, that is easily removed by sliding with a 100 nN load (fig. S4). This well-known "thermal film" is formed from adsorbed decomposition products of ZDDP (*15*, *24*). Typical thermal film thicknesses of ~10 nm were obtained after ~1 hour of heating the base stock bath, but can increase with time (*24*). After removing the thermal film with the tip, sliding is continued within the same region with a higher normal load to induce the growth of the tribofilm. The morphological evolution of the tribochemical products with increasing sliding cycles (one sliding cycle = a 1 × 1 $\mu m^2$ image) reveal randomly-located nucleation sites and subsequent growth of the sliding-induced tribofilm (Fig. 1). The tribofilm grows vertically and laterally (only within the region scanned at higher normal load) with further sliding, leading to a rough surface (movie S1). The total film volume increases linearly with sliding time during the first ~1200 cycles (Fig. 1, inset), indicating a zero-order reaction. The growth rate then increases rapidly, fitting well to a power law function, corresponding to an $n^{th}$ order reaction with $n$ = 0.22 (fig. S7), indicating a complex reaction pathway. The observed growth of a patchy film matches well with macroscopic results (*25*, *26*). Such macroscopic studies cannot make clear if the patchiness resulted from multiple asperities applying a range of loads at different locations, or by other means. As the loads and contact geometry are well-controlled in our single-asperity experiments, the heterogeneity is apparently intrinsic to the growth mechanism. This may indicate that nucleation is sensitively dependent on surface heterogeneities such as defects or roughness, and/or that there are instabilities in the growth mechanism, perhaps affected by stress, immediately after randomly-occurring nucleation events.

At these stresses (~4 GPa), the tribofilm growth rate was low, and the volume rarely reached a limiting value within the timeframe of our experiments (~10 hours), whereas growth typically saturates within a few hours in macroscopic experiments (*27*). This discrepancy may be due to the different sliding speeds (~80 $\mu$m/s for these AFM experiments vs. few mm/s up to m/s for macroscopic tests), or contact areas (on the order of 10-100 $nm^2$ in AFM vs. ~$10^9$ $nm^2$ for macroscopic tests), both of which reduce the area per unit time covered by AFM. The far larger amount of fluid exchange and the multi-asperity nature of the macroscopic contacts will also affect growth. Fortunately, AFM experiments performed at higher normal stresses (~6.5 GPa) enhanced the growth rate, and films reached a limiting height after prolonged sliding. We observe tribofilm wear once it reaches a thickness of ~30-40 nm, preventing further growth (fig. S5). At this thickness, there is no observable contrast in friction between the tribofilm and the surrounding substrate. However, before the tribofilm growth has saturated, a transient increase in friction is observed (fig. S10). Further study is required to determine if this effect is due to changes in tribofilm adhesion, modulus, roughness, or interfacial shear strength. However, the increase seen is consistent with macroscopic studies which report transient increases in friction for ZDDP-infused base stocks (*28*).

Within the sub-nanometer vertical resolution limits of our instrument, the tribofilms form without any observable wear of the iron oxide substrate. The proposed HSAB mechanism requires substantial plastic deformation and wear of the substrate (*18*). Considering the nanoscale dimensions of the nucleation centers observed in our experiments, the possibilities of cation exchange and digestion of atomic scale debris via molecular level mechanical mixing cannot be excluded. However, such a mechanism does not explain observations of similar macroscopic ZDDP tribofilms on other substrates such as DLC and silicon (*6*, *7*, *10*, *29*). Importantly, we also observe formation of tribofilms in AFM experiments using Si substrates with no Fe present (fig. S6) which are morphologically indistinguishable from those we form on Fe.

Our results also show that the tribofilm is not a product of sliding-induced transformation of the adsorbed thermal film, as growth occurs in regions where the thermal film was completely removed (fig. S4). Rather, these results indicate that tribofilm growth is fed by molecular species from solution into the contact zone, where tribochemical reactions occur.

Tribofilm growth rate and morphology were investigated as a function of normal load, which is directly related to the initial contact pressure (contact pressure at a fixed load will decrease as the compliant tribofilm's thickness increases). Multiple tribofilms were generated by sliding the AFM probe for 2000 sliding cycles at 100°C for a range of fixed loads (i.e., different initial contact pressures) (Fig. 2). Tri-

bofilm morphologies and volumes clearly reveal that growth is strongly affected by contact pressure. Beyond 5.2 ± 0.6 GPa, significant tribofilm deformation and pile-up is observed, indicating concurrent tribofilm generation and removal. This agrees with macroscopic observations and directly demonstrates the sacrificial property of ZDDP tribofilms beyond a critical thickness at the nanoscale (*30*).

The stress-dependent growth rate $\Gamma_{\text{growth rate}}$ ($nm^3/s$) fits well to a stress-activated Arrhenius model (Fig. 2):

$$\Gamma_{\text{growth rate}} = \Gamma_0 \exp\left(-\frac{\Delta G_{\text{act}}}{k_B T}\right) \quad (1)$$

where the pre-factor $\Gamma_0$ depends on the effective attempt frequency, $\Delta G_{\text{act}}$ is the free activation energy of the rate-limiting reaction in the growth process, $k_B$ is Boltzmann's constant, and $T$ the absolute temperature. The fit assumes that $\Delta G_{\text{act}}$ is influenced by stress according to:

$$\Delta G_{\text{act}} = \Delta U_{\text{act}} - \sigma \Delta V_{\text{act}} \quad (2)$$

where $\Delta U_{\text{act}}$ is the internal activation energy (energy barrier in the absence of stress), $\sigma$ is mean value of the stress component affecting the activation barrier (assumed to be the compressive contact pressure), and $\Delta V_{\text{act}}$ is the activation volume (*31*). The good fit suggests that tribofilm formation is an activated process (*31*). We find $\Delta U_{\text{act}}$ = 0.8 ± 0.2 eV and $\Delta V_{\text{act}}$ = 3.8 ± 1.2 $Å^3$, consistent with parameters for single atomic bond breaking or formation processes. The stress dependence suggests that the observed heterogeneous nucleation (Fig. 1) could result from surface roughness, which would lead to varying contact areas and stresses for a given normal load, lowering the energy barrier for the relevant tribochemical reaction where the local stress is higher.

Experiments performed as a function of temperature provide further support for an activated tribochemical reaction mechanism (Fig. 3). The volumetric growth rate of tribofilms generated by 5000 sliding cycles at ~4.4 GPa depended exponentially upon temperature. From fitting Eq. 1, we obtain $\Delta G_{\text{act}}$ = 0.62 ± 0.1 eV. Using the initial contact pressure determined from AFM force distance data and using $\Delta V_{\text{act}}$ from data in Fig. 2, we obtain $\Delta U_{\text{act}}$ = 0.74 ± 0.1 eV using Eq. 2, in excellent agreement with the value obtained from the stress-dependent data. This confirms the applicability of reaction rate theory by using independent stress and temperature dependent measurements. Our results provide a robust basis to support that the tribofilm growth occurs via stress- and thermally-activated tribochemical reactions, in contrast to previous empirical approaches (*25*). Our data do not provide any direct support for the HSAB model (*18*), which asserts that tribofilms can form even at contact pressures as low as 1 MPa where the entropy of mixing drives the reaction, not stress and temperature (*19*). The data are consistent with MD simulations showing that tribofilm formation can be driven by contact pressure (*8*). However, it is important to note that the simulation studies were performed on simpler zinc phosphate systems (with no sulfur), and effects of sliding were not investigated. Here we show directly using sliding experiments the role of pressure and temperature in forming tribofilms from ZDDP itself.

Ex situ chemical analysis using energy dispersive spectroscopy (EDS) and Auger electron spectroscopy (AES) identified the tribofilms' elemental composition. Point spectroscopy and elemental mapping using EDS (Fig. 4A) revealed clear signatures of Zn, S, and P inside the tribofilm (fig. S8), as expected from ZDDP-derived products (*32*). Much smaller peaks corresponding to P, S, and Zn were observed outside the tribofilm region, which are attributable to the thin (~10 nm), weakly bound thermal film (a significant fraction of which is likely dissolved during solvent rinsing prior to the EDS measurements). Elemental maps (Fig. 4A) reveal uniform distributions of P, S, and Zn inside the tribofilm. The Fe was uniform and indistinguishable between regions both inside and outside the tribofilm, further supporting that no significant wear or displacement of Fe was involved in tribofilm formation. AES, more surface-sensitive than EDS, revealed Zn, S, and P in the tribofilm region only (Fig. 4B). Far more Fe is seen outside the tribofilm, indicating little to no Fe is mixed in to the tribofilm itself.

The observed reduction of tribofilm robustness with increased thickness is consistent with reports that the modulus and hardness of macroscopic ZDDP tribofilms reduce with thickness (*20*). Furthermore, the contact pressure dependence of tribofilm formation reported here (Fig. 2) can explain the reported gradient in composition, structure, and mechanical properties of ZDDP tribofilms. Specifically, since the tribofilm has a lower modulus than the substrate, the contact stress at constant load reduces as the tribofilm thickens. This in turn reduces the amount of stress-induced cross-linking and other reactions that produce the tribofilm, resulting in a weaker, more compliant, graded structure and a further reduction in contact pressure. This feedback-driven self-limiting growth mechanism hinges on the stress-dependence of the thermally activated growth that we have uncovered (Fig. 2).

In summary, ZDDP antiwear tribofilm growth increases exponentially with applied pressure and temperature under single-asperity contact, in very good agreement with stress-assisted reaction rate theory; the kinetic parameters are consistent with a covalent bond reaction pathway. Repeated sliding at sufficiently high loads leads to abundant tribochemical reactions and the associated nucleation and growth of robust tribofilms with a pad-like structure similar to macroscopically-generated films. The tribofilm is not a product of the weakly adsorbed thermal film, but instead is generated from molecular species fed continuously into the contact zone. We confirm the sacrificial nature of the tribofilm beyond a threshold thickness, indicating that layers grown at lower applied pressures are weaker. The observations support that ZDDP's antiwear behavior derives from

mechanical protection provided by the tribofilm, as opposed to corrosion inhibition. We suggest that this in situ approach can be directly applied to understand further molecular-level tribochemical phenomena and functionality, such as the behavior of other important lubricant additives like friction modifiers, or for films formed in vapor-phase lubrication (*33*).

## REFERENCES AND NOTES


1. R. I. Taylor, Tribology and energy efficiency: From molecules to lubricated contacts to complete machines. *Faraday Discuss.* **156**, 361–382 (2012). Medline doi:10.1039/c2fd00122e

2. A. M. Barnes, K. D. Bartle, V. R. A. Thibon, A review of zinc dialkyldithiophosphates (ZDDPS): Characterisation and role in the lubricating oil. *Tribol. Int.* **34**, 389–395 (2001). doi:10.1016/S0301-679X(01)00028-7

3. H. Spikes, The history and mechanisms of ZDDP. *Tribol. Lett.* **17**, 469–489 (2004). doi:10.1023/B:TRIL.0000044495.26882.b5

4. E. S. Ferrari, K. J. Roberts, M. Sansone, D. Adams, A multi-edge X-ray absorption spectroscopy study of the reactivity of zinc di-alkyl-di-thiophosphates anti-wear additives. *Wear* **236**, 259–275 (1999). doi:10.1016/S0043-1648(99)00286-0

5. M. L. S. Fuller, M. Kasrai, G. M. Bancroft, K. Fyfe, K. H. Tan, Solution decomposition of zinc dialkyl dithiophosphate and its effect on antiwear and thermal film formation studied by X-ray absorption spectroscopy. *Tribol. Int.* **31**, 627–644 (1998). doi:10.1016/S0301-679X(98)00084-X

6. M. A. Nicholls, P. R. Norton, G. M. Bancroft, M. Kasrai, G. D. Stasio, L. M. Wiese, Spatially resolved nanoscale chemical and mechanical characterization of ZDDP antiwear films on aluminum-silicon alloys under cylinder/bore wear conditions. *Tribol. Lett.* **18**, 261–278 (2005). doi:10.1007/s11249-004-2752-9

7. B. Vengudusamy, J. H. Green, G. D. Lamb, H. A. Spikes, Tribological properties of tribofilms formed from ZDDP in DLC/DLC and DLC/steel contacts. *Tribol. Int.* **44**, 165–174 (2011). doi:10.1016/j.triboint.2010.10.023

8. N. J. Mosey, M. H. Müser, T. K. Woo, Molecular mechanisms for the functionality of lubricant additives. *Science* **307**, 1612–1615 (2005). Medline doi:10.1126/science.1107895

9. B. Vengudusamy, J. H. Green, G. D. Lamb, H. A. Spikes, Durability of ZDDP tribofilms formed in DLC/DLC contacts. *Tribol. Lett.* **51**, 469–478 (2013). doi:10.1007/s11249-013-0185-z

10. S. Equey, S. Roos, U. Mueller, R. Hauert, N. D. Spencer, R. Crockett, Reactions of zinc-free anti-wear additives in DLC/DLC and steel/steel contacts. *Tribol. Int.* **41**, 1090–1096 (2008). doi:10.1016/j.triboint.2008.03.004

11. G. C. Smith, Surface analytical science and automotive lubrication. *J. Phys. D* **33**, R187–R197 (2000). doi:10.1088/0022-3727/33/20/201

12. H. Spikes, Low- and zero-sulphated ash, phosphorus and sulphur anti-wear additives for engine oils. *Lubr. Sci.* **20**, 103–136 (2008). doi:10.1002/ls.57

13. K. T. Miklozic, J. Graham, H. Spikes, *Tribol. Lett.* **11**, 71 (2001). doi:10.1023/A:1016655316322

14. K. T. Miklozic, T. R. Forbus, H. A. Spikes, Performance of friction modifiers on ZDDP-generated surfaces. *Tribol. Trans.* **50**, 328–335 (2007). doi:10.1080/10402000701413505

15. M. A. Nicholls, T. Do, P. R. Norton, M. Kasrai, G. M. Bancroft, Review of the lubrication of metallic surfaces by zinc dialkyl-dithiophosphates. *Tribol. Int.* **38**, 15–39 (2005). doi:10.1016/j.triboint.2004.05.009

16. J. J. Habeeb, W. H. Stover, The role of hydroperoxides in engine wear and the effect of zinc dialkyldithiophosphates. *ASLE Trans.* **30**, 419–426 (1987). doi:10.1080/05698198708981775

17. F. Rounds, Effects of hydroperoxides on wear as measured in four-ball wear tests. *Tribol. Trans.* **36**, 297–303 (1993). doi:10.1080/10402009308983162

18. J. M. Martin, *Tribol. Lett.* **6**, 1–8 (1999). doi:10.1023/A:1019191019134

19. J. M. Martin, T. Onodera, C. Minfray, F. Dassenoy, A. Miyamoto, The origin of anti-wear chemistry of ZDDP. *Faraday Discuss.* **156**, 311–323 (2012). Medline doi:10.1039/c2fd00126h

20. S. Bec, A. Tonck, J. M. Georges, R. C. Coy, J. C. Bell, G. W. Roper, Relationship between mechanical properties and structures of zinc dithiophosphate anti-wear films. *Proc. R. Soc. London Ser. A* **455**, 4181–4203 (1999). doi:10.1098/rspa.1999.0497

21. S. Berkani, F. Dassenoy, C. Minfray, J.-M. Martin, H. Cardon, G. Montagnac, B. Reynard, Structural changes in tribo-stressed zinc polyphosphates. *Tribol. Lett.* **51**, 489–498 (2013). doi:10.1007/s11249-013-0188-9

22. D. Shakhvorostov, M. H. Müser, N. J. Mosey, D. J. Munoz-Paniagua, G. Pereira, Y. Song, M. Kasrai, P. R. Norton, On the pressure-induced loss of crystallinity in orthophosphates of zinc and calcium. *J. Chem. Phys.* **128**, 074706 (2008). doi:10.1063/1.2837809

23. See supplementary materials on *Science* Online.

24. M. Aktary, M. T. McDermott, J. Torkelson, Morphological evolution of films formed from thermooxidative decomposition of ZDDP. *Wear* **247**, 172–179 (2001). doi:10.1016/S0043-1648(00)00525-1

25. H. Fujita, H. A. Spikes, Study of zinc dialkyldithiophosphate antiwear film formation and removal processes, part II: Kinetic model. *Tribol. Trans.* **48**, 567–575 (2005). doi:10.1080/05698190500385187

26. M. Aktary, M. T. McDermott, G. A. McAlpine, Morphology and nanomechanical properties of ZDDP antiwear films as a function of tribological contact time. *Tribol. Lett.* **12**, 155–162 (2002). doi:10.1023/A:1014755123184

27. H. Fujita, R. P. Glovnea, H. A. Spikes, Study of zinc dialkydithiophosphate antiwear film formation and removal processes, part I: Experimental. *Tribol. Trans.* **48**, 558–566 (2005). doi:10.1080/05698190500385211

28. B. Kim, R. Mourhatch, P. B. Aswath, Properties of tribofilms formed with ashless dithiophosphate and zinc dialkyl dithiophosphate under extreme pressure conditions. *Wear* **268**, 579–591 (2010). doi:10.1016/j.wear.2009.10.004

29. M. Burkinshaw, A. Neville, A. Morina, M. Sutton, Calcium sulphonate and its interactions with ZDDP on both aluminium-silicon and model silicon surfaces. *Tribol. Int.* **46**, 41–51 (2012). doi:10.1016/j.triboint.2011.06.014

30. Y. R. Li, G. Pereira, M. Kasrai, P. R. Norton, The effect of steel hardness on the performance of ZDDP antiwear films: A multi-technique approach. *Tribol. Lett.* **29**, 201–211 (2008). doi:10.1007/s11249-008-9297-2

31. T. D. B. Jacobs, R. W. Carpick, Nanoscale wear as a stress-assisted chemical reaction. *Nat. Nanotechnol.* **8**, 108–112 (2013). doi:10.1038/nnano.2012.255

32. A. Morina, A. Neville, Tribofilms: Aspects of formation, stability and removal. *J. Phys. D* **40**, 5476–5487 (2007). doi:10.1088/0022-3727/40/18/S08

33. A. L. Barnette, D. B. Asay, J. A. Ohlhausen, M. T. Dugger, S. H. Kim, Tribochemical polymerization of adsorbed n-pentanol on SiO2 during rubbing: When does it occur and is it responsible for effective vapor phase lubrication? *Langmuir* **26**, 16299–16304 (2010). Medline doi:10.1021/la101481c

34. J. E. Sader, J. W. Chon, P. Mulvaney, Calibration of rectangular atomic force microscope cantilevers. *Rev. Sci. Instrum.* **70**, 3967 (1999). doi:10.1063/1.1150021

35. L. Dongmo, J. S. Villarrubia, S. N. Jones, T. B. Renegar, M. T. Postek, J. F. Song, Experimental test of blind tip reconstruction for scanning probe microscopy. *Ultramicroscopy* **85**, 141–153 (2000). doi:10.1016/S0304-3991(00)00051-6

36. K. L. Johnson, *Contact Mechanics* (Cambridge Univ. Press, Cambridge, 1987).

37. B. Luan, M. O. Robbins, The breakdown of continuum models for mechanical contacts. *Nature* **435**, 929–932 (2005). Medline doi:10.1038/nature03700

38. C. Donnet, A. Erdemir, *Tribology of Diamond-Like Carbon Films: Fundamentals and Applications* (Springer, New York, 2008).

39. M. A. Nicholls, P. R. Norton, G. M. Bancroft, M. Kasrai, T. Do, B. H. Frazer, G. De Stasio, Nanometer scale chemomechanical characterization of antiwear films. *Tribol. Lett.* **17**, 205–216 (2004). doi:10.1023/B:TRIL.0000032447.32442.6a

40. K. Demmou, S. Bec, J. L. Loubet, J. M. Martin, Temperature effects on mechanical properties of zinc dithiophosphate tribofilms. *Tribol. Int.* **39**, 1558–1563 (2006). doi:10.1016/j.triboint.2006.01.025

41. M. A. Nicholls, T. Do, P. R. Norton, G. M. Bancroft, M. Kasrai, T. W. Capehart, Y.-T. Cheng, T. Perry, Chemical and mechanical properties of ZDDP antiwear films on steel and thermal spray coatings studied by XANES spectroscopy and nanoindentation techniques. *Tribol. Lett.* **15**, 241–248 (2003). doi:10.1023/A:1024813203442

42. E. Reedy, Thin-coating contact mechanics with adhesion. *J. Mater. Res.* **21**, 2660–2668 (2006). doi:10.1557/jmr.2006.0327

## ACKNOWLEDGMENTS

This work was supported by the University of Pennsylvania, School of Engineering and Applied Sciences, and the National Science Foundation under grant CMMI-1200019. The authors acknowledge the use of University of Pennsylvania Nano/Bio Interface Center Facilities and the Nanoscale Characterization Facility in the Singh Center for Nanotechnology. We acknowledge Evans Analytical Group (East Windsor, NJ) for AES measurements, and ExxonMobil's Corporate Strategic Research (CSR) laboratory for providing materials and financial support. We thank Mr. Qizhan Tam for Matlab analysis and Dr. Tevis D.B. Jacobs for transmission electron microscopy analysis of AFM probes. F.M. acknowledges support from the Marie Curie International Outgoing Fellowship for Career Development within the 7th European Community Framework Programme under Contract No. PIOF-GA-2012-328776. We acknowledge funding from the Nanotechnology Institute through the Ben Franklin Technology Development Authority (BFTDA). The authors gratefully acknowledge helpful discussions with Prof. Andrew Jackson.

## SUPPLEMENTARY MATERIALS

www.sciencemag.org/cgi/content/full/science.1258788/DC1
Materials and Methods
Supplementary Text
Figs. S1 to S10
Movie S1
References (*34*–*42*)

15 July 2014; accepted 27 February 2015
Published online 12 March 2015
10.1126/science.1258788

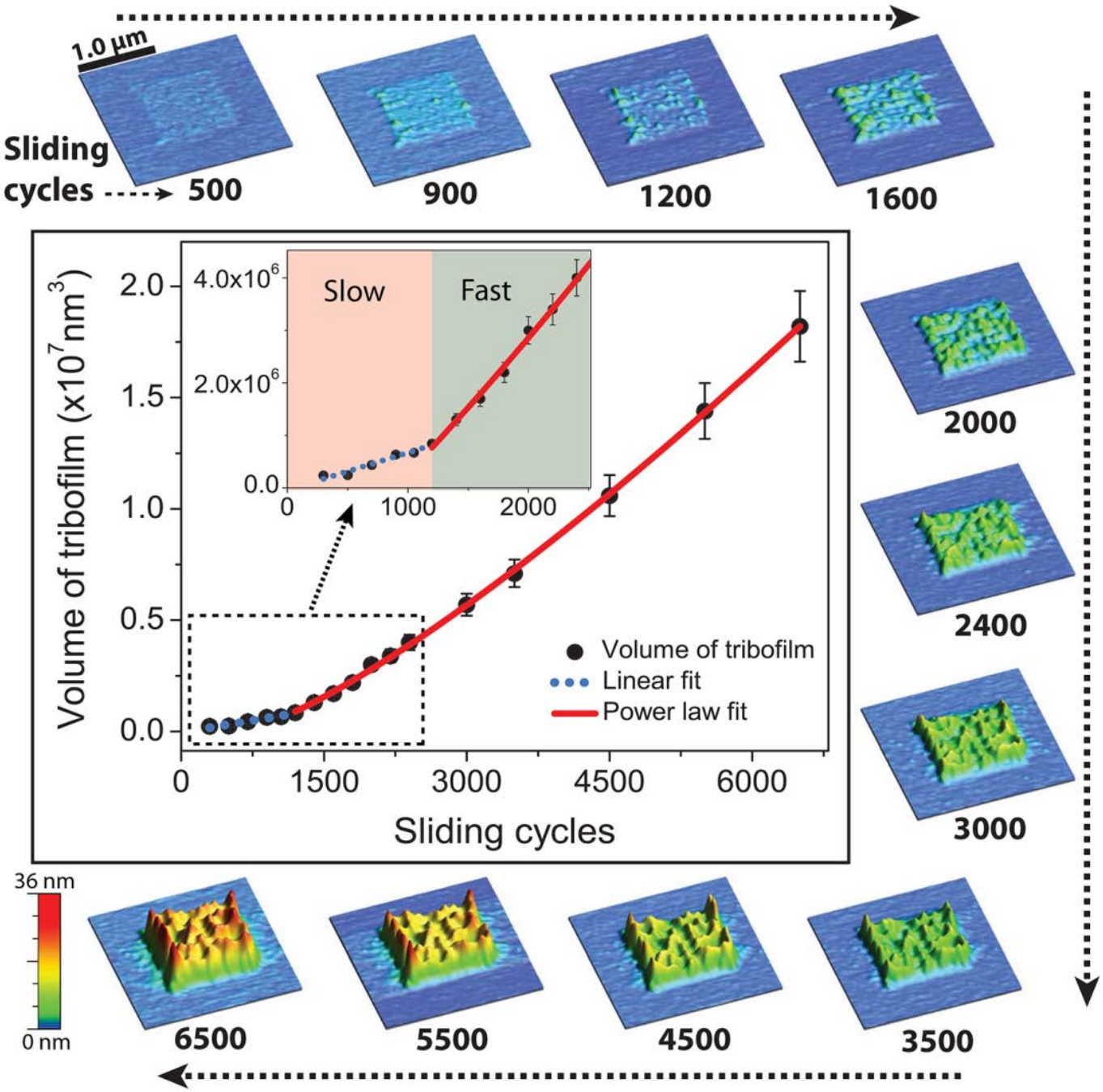


**Fig. 1. Morphology and volumetric growth of tribofilm.** Tribofilm volume (Mean ± SD) vs. sliding cycles, with linear and power law fits to the initial and subsequent growth regimes, respectively. Inset: zoom-in of the initial growth period. Around the perimeter, clockwise from upper left: periodically-acquired 2 × 2 µm$^2$ AFM images of an iron oxide surface using a DLC-coated silicon AFM tip immersed in ZDDP-containing base stock, acquired at a non-perturbative load of 20 ± 0.1 nN. Below each image, the number of previously-acquired 1 × 1 µm$^2$ scans ("sliding cycles") at a load of 340 ± 2.0 nN (4.2 ± 0.5 GPa) are indicated. The images demonstrate progressive tribofilm growth where the higher load was applied.

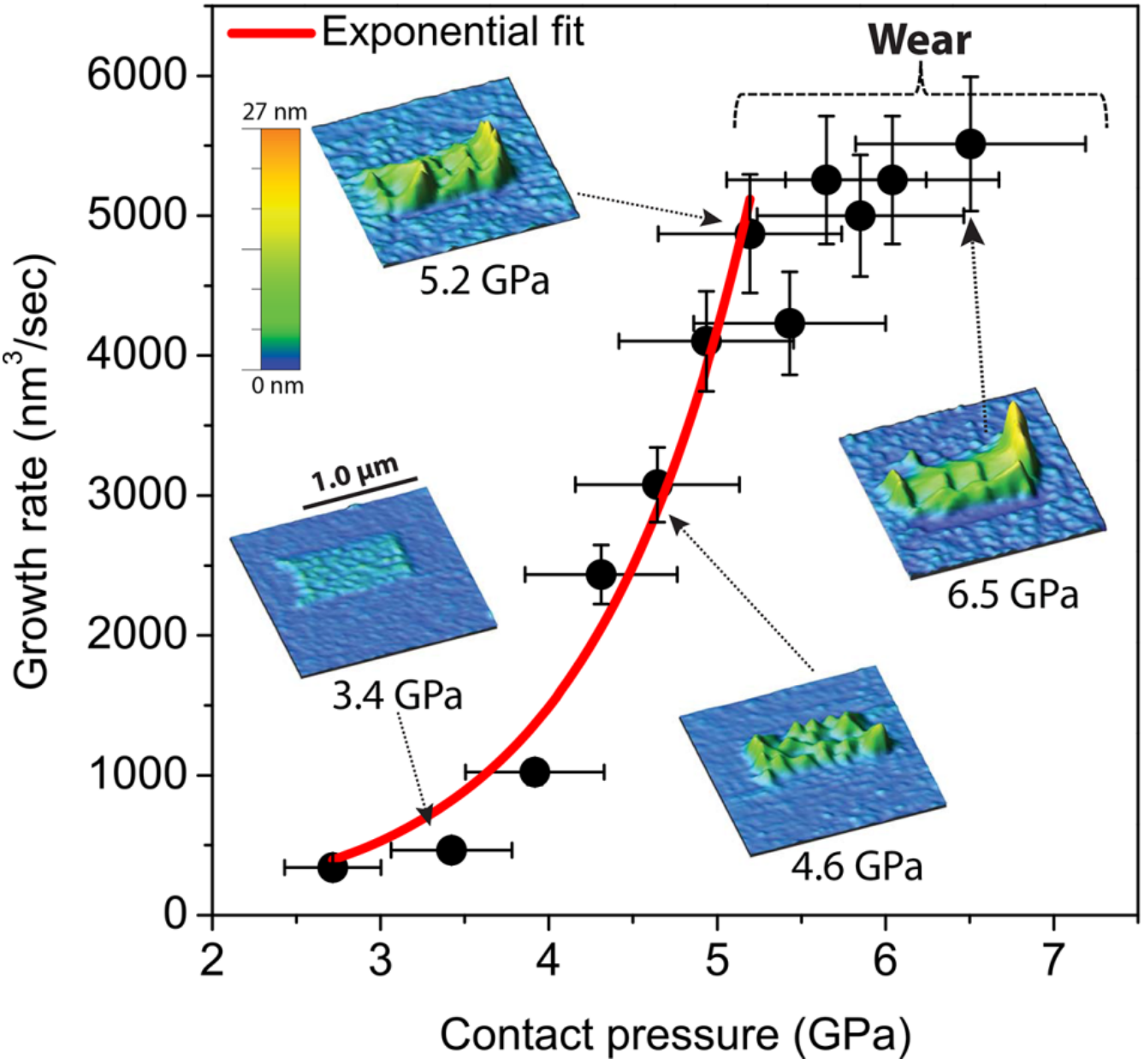


**Fig. 2. Tribofilm volumetric growth rate dependence on contact pressure.** Tribofilm growth rate (Mean ± SD) is exponential at low stresses (Mean ± SD). Further growth is inhibited above ~5 GPa as the tip wears away newly deposited material. The selection of 2 × 2 $\mu m^2$ topographic contact mode AFM images shown are acquired at a non-perturbative load after generating tribofilms in the central 1.0 × 0.5 $\mu m^2$ regions at various contact pressures.

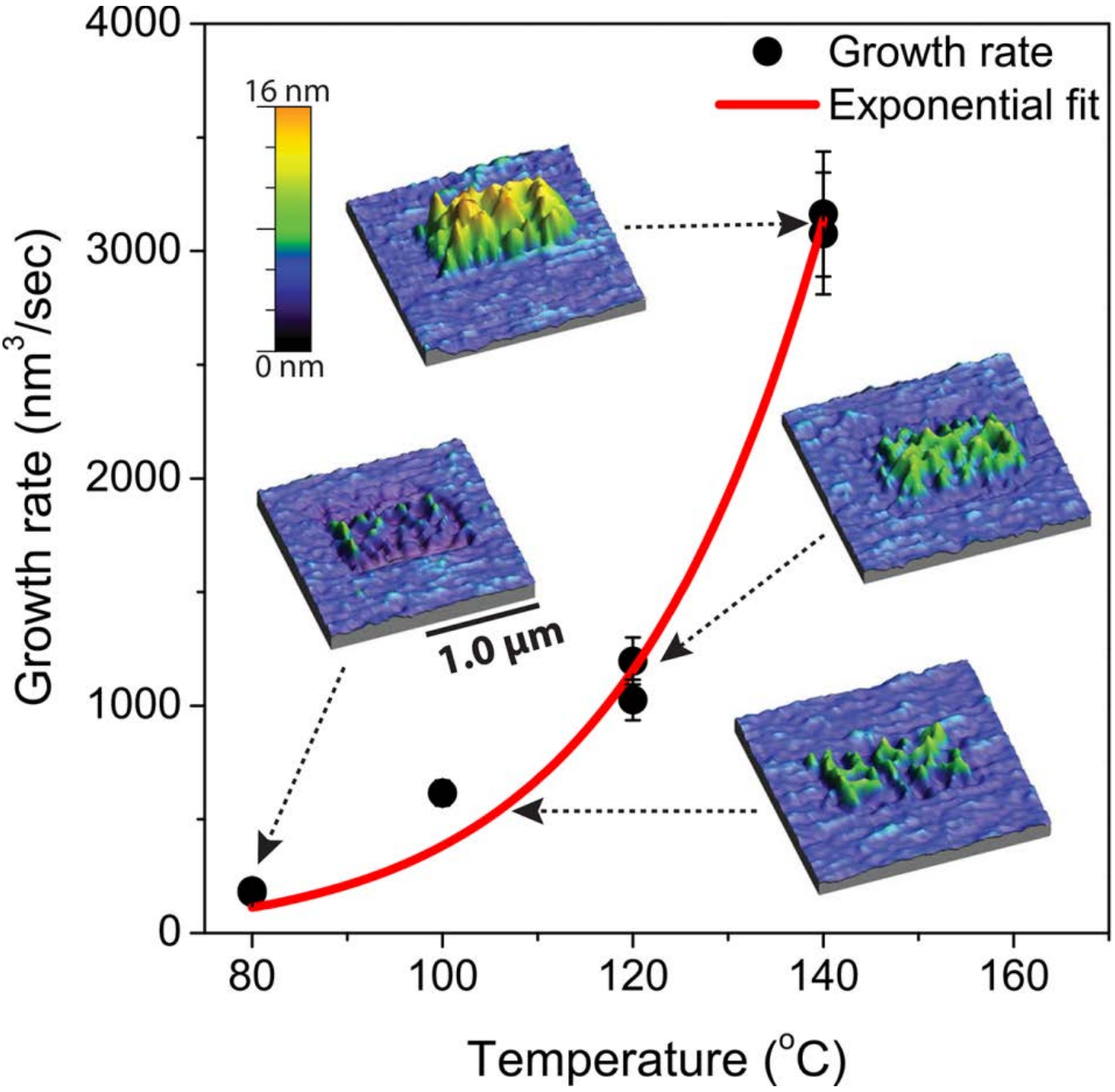


**Fig. 3. Tribofilm volumetric growth rate dependence on temperature.** Growth rate (Mean ± SD) vs. temperature data fitted with an exponential function (Eq. 1). The selection of 2 × 2 µm$^2$ topographic contact mode AFM images shown are acquired at a non-perturbative load after generating tribofilms in the central 1.0 × 0.5 µm$^2$ regions at 80°C, 100°C, 120°C and 140°C at a contact stress of ~4.4 GPa.

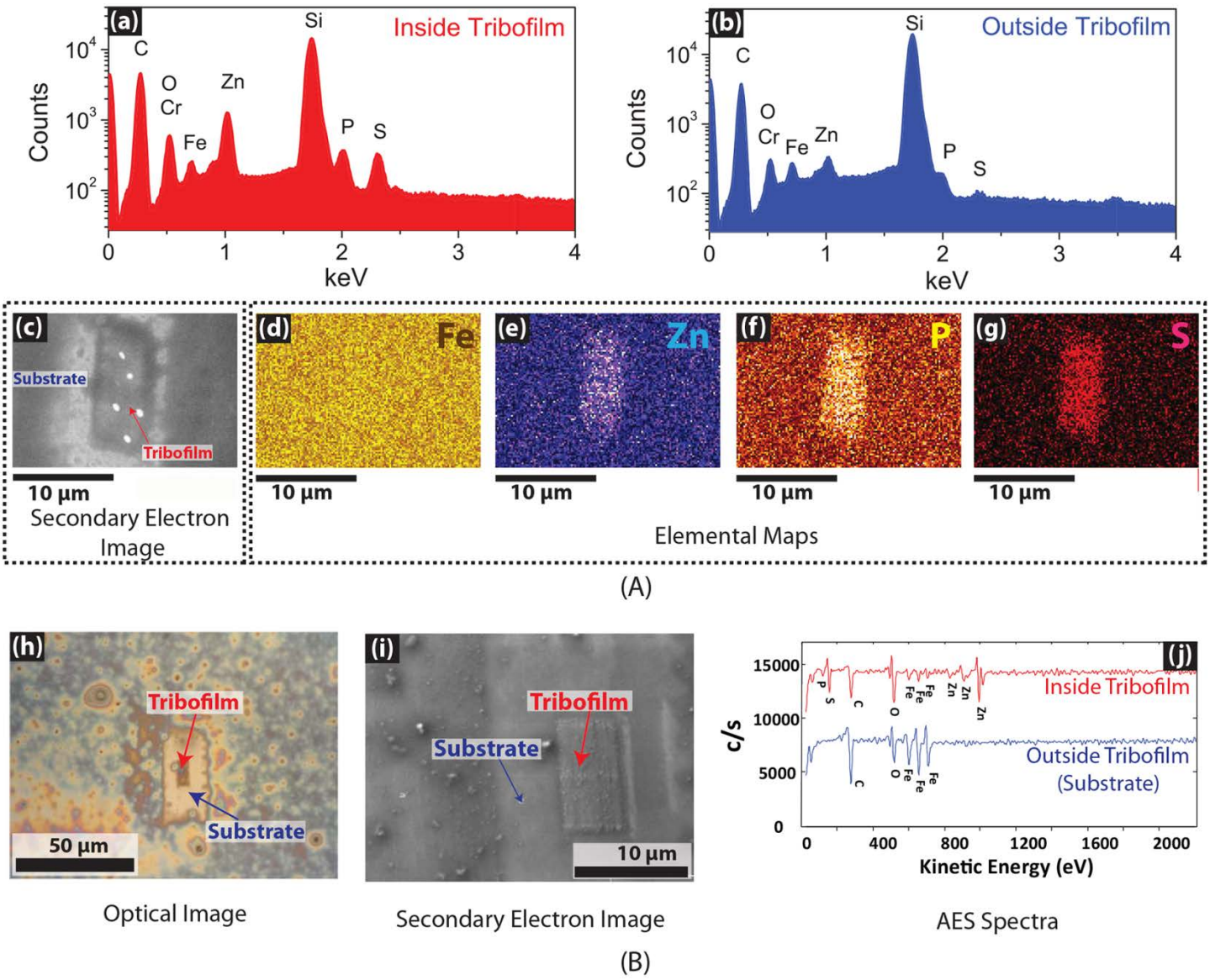


**Fig. 4. Ex situ chemical characterization.** (**A**) EDS point spectra (estimated sampling depth of ~ 1µm), acquired for regions (a) inside and (b) outside the tribofilm, i.e., for the portion of the substrate covered with the thermal film. (c) Secondary electron image of the 10 × 5.0 µm$^2$ tribofilm shown on the bottom left. Corresponding elemental maps for (d) Fe, (e) Zn, (f) P, and (g) S. (**B**) (h) Optical and (i) secondary electron image of a 10 × 5.0 µm$^2$ tribofilm obtained using scanning AES. (j) AES spectra for the tribofilm and the substrate (estimated sampling depth of ~ 3 nm).